Optics Letters

Time reflection and refraction of graphene plasmons at a temporal discontinuity

Galaad Altares Menendez* and Bjorn Maes

Micro- and Nanophotonic Materials Group, University of Mons, 20 Place du Parc, B-7000 Mons, Belgium
**Corresponding author: Galaad.AltaresMenendez@umons.ac.be*

Received 5 October 2017; revised 2 November 2017; accepted 3 November 2017; posted 6 November 2017 (Doc. ID 308602); published 30 November 2017

A dynamical change of material properties induces a special type of reflection and refraction at a temporal discontinuity. Here, we study the interaction of graphene plasmons with single and double temporal discontinuities or shocks, leading to controlled in-plane scattering. We analytically determine the Fresnel-like coefficients for graphene plasmons at these boundaries, and validate our results by rigorous numerical simulations. Temporally controlled doping of two-dimensional materials such as graphene thus leads to a new mechanism for planar and compact plasmonic devices.

OCIS codes: (250.5403) Plasmonics; (130.7405) Wavelength conversion devices; (320.5540) Pulse shaping.

https://doi.org/10.1364/OL.42.005006

Graphene plasmonics has gained much attention, because the particular plasmons are widely tunable, show extreme confinement, and suffer relatively low losses [1–3]. In parallel studies, dynamical modulation of materials was shown to provide for a broad variety of unusual phenomena such as wavelength conversion [4–9], optical isolation [10,11], and topological effects [12,13]. In this context, the behavior of electromagnetic waves incident on "time boundaries" has been known for a long time [14], and these phenomena are very general, as a recent implementation of time reflection for water waves illustrates [15].

However, guided optical modes (such as plasmons) with discontinuities have not yet been addressed, to the best of our knowledge. Therefore, in this Letter, we merge the fields of time boundaries with graphene plasmons, leading to an interesting way to reflect plasmons in two-dimensional compact circuits. These plasmons are highly suitable for this application, as the Fermi level can be modulated rapidly. Additionally, the nature of the plasmonic modes leads to straightforward expressions for the reflection and transmission properties at single or double discontinuities (so-called temporal slabs). Importantly, the phenomena and the analysis we report are general and valid for other types of guided modes.

We study plasmons propagating in a graphene sheet incident on two types of time boundaries: a single time step [Fig. 1(a)] and a double time step [or slab, Fig. 1(b)]. The phenomenon at a single time step is sketched in [Fig. 1(c)]: a forward propagating plasmonic mode (or pulse) is split into a backward (reflected) and forward (transmitted) wave after the shock (an abrupt change of E_F [16]).

Here, the time boundaries are abrupt changes in the Fermi level E_F of the graphene sheet. We employ a Drude-like model for the graphene conductivity [17]:

$$\sigma(\omega) = \frac{e^2 E_F}{\pi\hbar^2}\frac{j}{\omega + j\tau_{\mathrm{gra}}^{-1}}, \tag{1}$$

which is valid for $E_F \gg k_B T$, with $k_B T \approx 0.026$ eV. Since this conductivity only takes into account intraband transitions, we also require that $\hbar\omega \ll 2E_F$. Close to a time interface (thus without long propagation), we can ignore the losses $\tau_{\mathrm{gra}}^{-1} = 0$. However, the phenomena remain even with losses, as they do not depend on the mode amplitude.

The graphene plasmon dispersion in the nonretarded regime ($\beta \gg \omega/c$ with β the mode propagation constant) directly depends on E_F [18]:

$$\mathrm{Re}(\beta) = \frac{2\varepsilon_0\varepsilon_r\pi\hbar^2\omega^2}{e^2 E_F}, \tag{2}$$

with ε_r the permittivity of the surrounding medium (we use $\varepsilon_r = 1$).

Since the time derivatives of the electric displacement $\boldsymbol{D}$ and magnetic induction $\boldsymbol{B}$ appear in Maxwell's equations, $\boldsymbol{D}$ and $\boldsymbol{B}$ must be continuous at a time interface at time $t = 0$ [19,20]:

$$\boldsymbol{D}(t = 0^-) = \boldsymbol{D}(t = 0^+), \qquad \boldsymbol{B}(t = 0^-) = \boldsymbol{B}(t = 0^+). \tag{3}$$

Here, graphene is modeled with a sheet current $\boldsymbol{J}$, so Maxwell's equations read

$$\nabla \times \boldsymbol{E} = -\frac{\partial \boldsymbol{B}}{\partial t}, \qquad \nabla \times \boldsymbol{H} = \frac{\partial \boldsymbol{D}}{\partial t} + \boldsymbol{J}. \tag{4}$$

We consider a constant permittivity and permeability in the surrounding medium, so there the electric field $\boldsymbol{E}$ and magnetic field $\boldsymbol{H}$ are continuous. Moreover, in a dispersive medium such as graphene, $\boldsymbol{E}$ and $\boldsymbol{H}$ are also continuous [21], so Eq. (3) reduces to temporal continuity of $\boldsymbol{E}$ and $\boldsymbol{H}$. Graphene plasmons, being transverse magnetic modes, are easily described by their

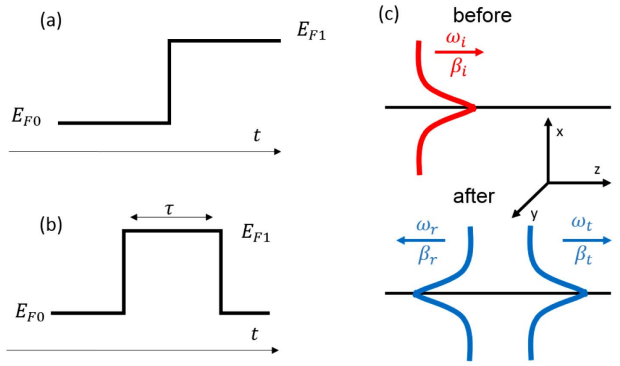

Fig. 1. (a) Time step and (b) slab. (c) Step effect: an incident plasmon generates a reflected and transmitted plasmon at a different frequency.

transverse magnetic component (here along y). Using continuity of H (and convention $e^{-j\omega t}$),

$$H_{i,y}^{(\omega_i)} h_{i,y}^{(\omega_i)}(x) e^{j\beta_i z} = H_{r,y}^{(\omega_r)} h_{r,y}^{(\omega_r)}(x) e^{j\beta_r z} + H_{t,y}^{(\omega_t)} h_{t,y}^{(\omega_t)}(x) e^{j\beta_t z}, \tag{5}$$

where $H_{\alpha,y}^{(\omega_\alpha)}$ is the mode amplitude, $h_{\alpha,y}^{(\omega_\alpha)}(x)$ the mode profile, and β the propagation constant. Superscripts (ω_α) indicate the frequency, and subscripts $\alpha = i, r, t$ stand for the incident, reflected, or transmitted. At a regular spatial interface (a change of index in space), the frequency is conserved across the spatial discontinuity. In contrast, for a temporal discontinuity, the wavevector is conserved [22]: the z dependence in Eq. (5) imposes that all the propagation constants β_α are equal:

$$\beta_i = \beta_t = \beta_r. \tag{6}$$

Since we change the Fermi level at the time interface, the frequency of the incident mode has to adapt to keep the wavevector unchanged [Eq. (2) and Fig. 2]. Consequently, when an incident mode with a propagation constant β_i is incident on a time boundary (when the medium suddenly changes), it produces a reflected and a transmitted ("refracted") mode with the same propagation constants (β_r, β_t), but at a different frequency. Using the dispersion [Eq. (2)], we link the frequencies to the Fermi levels around the temporal interface:

$$\gamma\omega_i = \omega_t = -\omega_r, \tag{7}$$

where ω_i, ω_r, and ω_t are the incident, reflected and transmitted frequencies, respectively. The minus sign accounts for backward propagation. $\gamma = \sqrt{E_{F1}/E_{F0}}$ is the shock amplitude, with E_{F0} (E_{F1}) the Fermi level before (after) the time boundary.

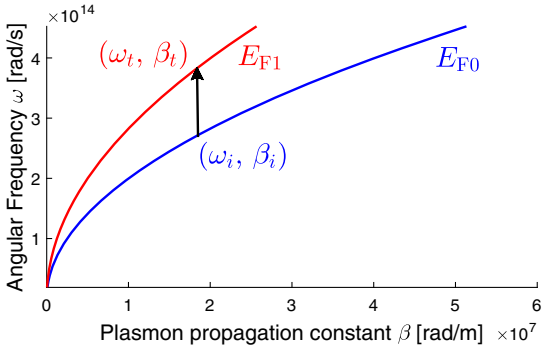

Fig. 2. Time step and plasmon dispersion: the propagation constant is conserved, while the frequency changes. Here, $E_{F1} > E_{F0}$.

Since β is conserved, and we are in the nonretarded regime, the plasmonic mode profiles $h_{\alpha,y}^{(\omega)}(x)$ are very similar on both sides of the temporal interface. This is why we cancel them out in the remainder (using the same normalization $h_{\alpha,x}^{(\omega_\alpha)}(0^+) = 1$), which is a very useful approximation stemming from the extreme confinement of graphene plasmons. For lower-index modes, this assumption should be reconsidered. We define the Fresnel-like reflection and transmission coefficients as

$$H_{r,y}^{(\omega_r)} = r_{\text{step}} H_{i,y}^{(\omega_i)}, \qquad H_{t,y}^{(\omega_t)} = t_{\text{step}} H_{i,y}^{(\omega_i)}. \tag{8}$$

By further imposing the continuity of the time derivative of $\boldsymbol{H}$ [see Eq. (4), as $\nabla \times \boldsymbol{E}$ is continuous everywhere, except at $x = 0$] in Eq. (5), one finds

$$-j\omega_i e^{j\beta_i z} = j\omega_r r_{\text{step}} e^{j\beta_r z} - j\omega_t t_{\text{step}} e^{j\beta_t z}. \tag{9}$$

Combining Eqs. (5)–(9), the transmittance and reflectance become

$$T_{\text{step}} = |t_{\text{step}}|^2 = \left(\frac{\gamma+1}{2\gamma}\right)^2, \qquad R_{\text{step}} = |r_{\text{step}}|^2 = \left(\frac{\gamma-1}{2\gamma}\right)^2. \tag{10}$$

A slab time profile consists of two successive time steps [Fig. 1(b)], so that with the step coefficients and the phase picked up between,

$$R_{\text{slab}} = \frac{1}{4}(\gamma - \gamma^{-1})^2 \sin^2(\gamma\omega\tau), \qquad T_{\text{slab}} = 1 + R_{\text{slab}}, \tag{11}$$

with τ the slab time duration and ω the incident (and transmitted) angular frequency. It is interesting to note that in the case of a spatial slab, interferences occur because of a phase βl (with l the slab length), whereas here the phase is described $\gamma\omega\tau$ (with τ the slab duration and $\gamma\omega$ the frequency "inside" the slab).

Equations (10) and (11) describe graphene plasmons at time steps and slabs. Before interpreting these results, we examine how the energy of the modes is affected, which allows for a better comparison with simulations. Using the Poynting vector, we can define the total incident energy. The power (per unit y-length) at a given frequency for TM polarization is

$$P_\alpha^{(\omega)} = \frac{1}{2}|H_{\alpha,y}^{(\omega)}|^2 \int h_{\alpha,y}^{*(\omega)}(x) e_{\alpha,x}^{(\omega)}(x)\mathrm{d}x = \frac{1}{2\omega\varepsilon_0}|H_{\alpha,y}^{(\omega)}|^2, \tag{12}$$

where $e_{\alpha,x}^{(\omega)}$ and $h_{\alpha,y}^{(\omega)}$ are the E and H mode profiles. We used $h_{\alpha,y}^{(\omega)}(x) = e^{-\kappa|x|}$, $e_{\alpha,x}^{(\omega)} = \beta/(\omega\varepsilon_0) h_{\alpha,y}^{(\omega)}$, and $\kappa \simeq \beta$ for high-index modes. Then we can define the energy U_α of a pulse (per unit y-length) as

$$U_\alpha = \int P_\alpha^{(\omega)} \mathrm{d}\omega \simeq \int \frac{1}{2\omega\varepsilon_0}|H_{\alpha,y}^{(\omega)}|^2 \mathrm{d}\omega. \tag{13}$$

In Eq. (8), we defined

$$R_{\text{step}} = |H_{r,y}^{(\omega_r)}|^2/|H_i^{(\omega_i)}|^2, \quad T_{\text{step}} = |H_{t,y}^{(\omega_t)}|^2/|H_i^{(\omega_i)}|^2. \tag{14}$$

Using these relations, along with Eq. (13), one can show that the pulse energies are immediately quantified by our coefficients:

$$R_{\text{step}} = U_r/U_i, \qquad T_{\text{step}} = U_t/U_i, \tag{15}$$

where U_i, U_r, and U_t are the incident, reflected, and transmitted energies, respectively. Note that the power fraction for monochromatic waves includes a factor γ: $P_t^{(\omega_t)}/P_i^{(\omega_i)} = T_{\text{step}}/\gamma$,

whereas Eq. (15) does not. Indeed, the pulses experience a stretching of the envelope [19], described by a factor γ.

For the temporal slab, since the transmittance T_{slab} and reflectance R_{slab} are frequency dependent, the energy conservation at the interface needs to be calculated as

$$\int R_{\text{slab}}(\omega)P_i^{(\omega)}\mathrm{d}\omega = U_r, \qquad \int T_{\text{slab}}(\omega)P_i^{(\omega)}\mathrm{d}\omega = U_t. \quad \textbf{(16)}$$

Therefore, because of the specific graphene plasmon dispersion, we can directly interpret the analytical reflectance and transmittance in terms of energy for both steps and slabs (even if the frequency changes for steps).

We run finite element method (FEM) simulations [23] to validate our results. We model the carrier density by a step function, which is an approximation, but this avoids the use of microscopic transport equations for the graphene electrons. We record (in time domain) the field profiles at two specific points in space, and then separate incident, reflected, and transmitted pulses. When there are multiple reflected or transmitted pulses, the Fresnel coefficients are obtained by integrating the fields of all pulses. The simulations of a step interface (Fig. 3) from $E_{\text{F0}} = 0.6$ eV to $E_{\text{F1}} = 0.36$ eV ($\gamma = 0.77$) show that the reflected and transmitted plasmons indeed have a different frequency, in accordance with Eq. (7). The simulations agree well with the theory [Eq. (10)]: $r_{\text{th}} = 0.1455$, $r_{\text{FEM}} = 0.1452$, $t_{\text{th}} = 1.1455$, and $t_{\text{FEM}} = 1.1454$. (Note that the coefficients are frequency-independent for steps.) In this case, energy is injected in the system, as we will comment on later. We remark also that the spectrum of the pulse is compressed by a factor γ. Since an abrupt step does not take into account potential carrier dynamic delays, the inset of Fig. 3 shows simulations with a "smoother" transition. One notices that the transmission stays similar, while the reflection decreases. However, a variation of graphene on a scale of 10 fs was demonstrated [24–26], so our abrupt model produces similar values to more realistic transitions.

For the slab interface, we compare Eq. (11) to FEM simulations in Fig. 4 for various time slabs (varying τ). The numerical results (lines) are in good agreement with the theory (open circles). This shows that energy is injected into the plasmon, since the transmittance is always greater than one. Furthermore, a significant reflectance is possible (e.g., R can be 100% when $\gamma = \sqrt{2} \pm 1$, and even larger for other γ).

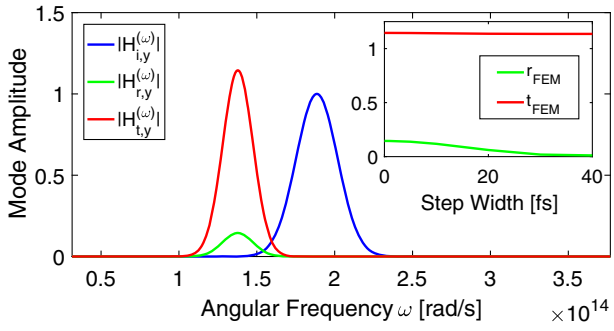

Fig. 3. Simulated incident (blue), reflected (green), and transmitted (red) H fields in the frequency domain for a time step. The amplitudes are normalized to the maximum incident amplitude. The inset shows the evolution of FEM calculated transmission t_{FEM} and reflection r_{FEM} coefficients as a function of the time interface width.

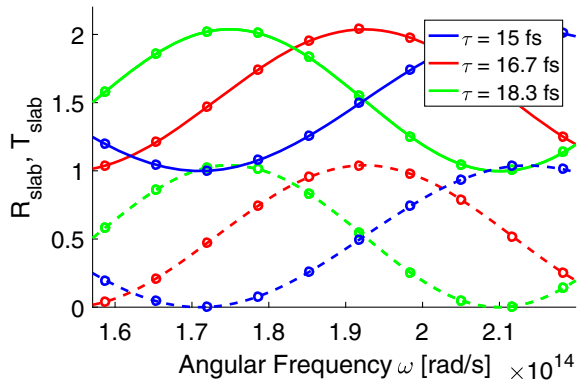

Fig. 4. Comparison between the slab model [Eq. (11), open circles] and FEM simulations (dashed for R and solid lines for T) for various slab durations τ. Here, $\gamma = 2.45$ (corresponding to $E_{F0} = 0.1$ eV, and $E_{F1} = 0.6$ eV).

The oscillations in transmittance and reflectance correspond to interferences between the plasmons reflected and transmitted at both interfaces (steps) of the slab.

Figure 5 shows simulated snapshots of a plasmon pulse at a temporal slab, visualizing clearly the reflection and transmission effects. In this case, energy is injected in the system ($T_{\text{slab}} = 2.02$ and $R_{\text{slab}} = 1.02$ at the central incident frequency ω_0). Notice also the dispersion effects: modes with a lower β (thus a higher effective wavelength) propagate faster in graphene sheets [see the leading edge of the "transmitted" pulse, Fig. 5(c)]. In contrast, the reflected pulse is the same as the incident pulse, showing the dispersion compensation [15]. Note that the simulations are spatially two-dimensional (x, z), but we only show the field along the sheet, as radiation is negligible because of the large impedance mismatch.

Now we discuss the parameter dependencies of steps and slabs using our model, since the simulations are in good agreement. For a step, the only available parameter is the shock amplitude γ [see Eq. (10)]. Surprisingly, the specific start and end Fermi level, and the incident plasmon frequency, do not play a role: the only relevant parameter is the ratio $E_{\text{F1}}/E_{\text{F0}}$. It may seem that high γ values are difficult to achieve in practice, but this is feasible if one starts from a low E_{F0}. Figure 6 represents the transmittance and reflectance [which directly corresponds to the energies [see Eq. (15)] as a function

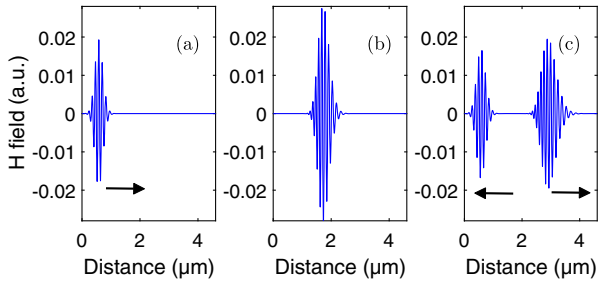

Fig. 5. Simulations for a plasmonic pulse with a time slab. The central incident frequency is $\omega_0 = 2\pi 30 \times 10^{12}$ rad/s, $\tau = \pi/\omega_0$; the plasmon period is $T_p = 2\pi/\omega_0$, and the shock happens at $t = 0$. The profile along the sheet is shown at time: (a) $-20T_p$, (b) 0, and (c) $20T_p$. We used $E_{\text{F0}} = 0.1$ eV and $E_{\text{F1}} = 0.6$ eV.

of γ at a step. Energy is injected (reduced) in the forward propagating pulse for shocks with $\gamma < 1$ (>1). This profile is somewhat similar to the transmission (not transmittance) of spatial interfaces in a function of the index fraction n_2/n_1.

In contrast, the slab characteristics depend on the length τ, the amplitude γ, and the incident frequency ω. These parameters allow for a large tunability; see Figs. 7(a) and 7(b). The slab transmittance is always greater than one, and this forward energy injection is frequency dependent. The maximum transmittance (thus, also reflectance) is the same for γ and γ^{-1}, as seen in Eq. (11). A larger shock (γ more distant from 1) leads to an overall higher transmittance, but interference gives oscillations [Fig. 7(a)]. For the same reason, the slab length allows tuning of the reflectance and transmittance [Fig. 7(b)]. This mechanism thus provides plasmon amplification, perhaps leading to loss compensation [27]. Note also that R_{slab} is fairly large in comparison with R_{step}. This is because a slab consists of two steps with amplitudes γ and γ^{-1}, and the intricate interference leads to adding $r^{(\gamma)}_{\text{step}} t^{(1/\gamma)}_{\text{step}}$ with $t^{(\gamma)}_{\text{step}} r^{(1/\gamma)}_{\text{step}}$.

In these effects, the Fermi level variation occurs within a time comparable to the graphene plasmon period, which is experimentally challenging. One could use lower frequency graphene plasmons to lift this limitation. One may also use a longer slab duration, leading to more oscillations in the transmittance. In the end, if the transmittance oscillates many times in the pulse bandwidth, it is expected that the system will experience an average (increased) transmittance for the whole pulse. In order to achieve ultrafast switching, one can consider a direct external pump to excite carriers on a timescale faster than the electron relaxation time (on the order of 10^{-12} s). Alternatively, one could exploit nonlinear Kerr-type effects, or switch to other two-dimensional materials [28].

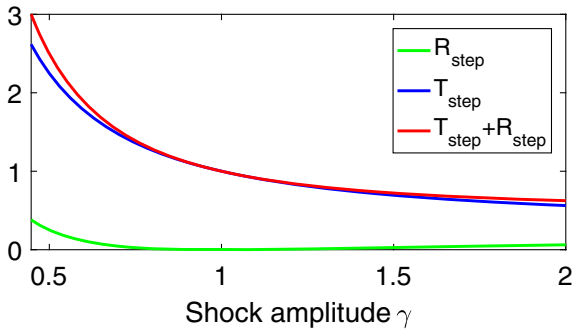

Fig. 6. Transmittance and reflectance by a time step. Energy is injected for steps with $\gamma < 1$ [see Eqs. (10) and (15)].

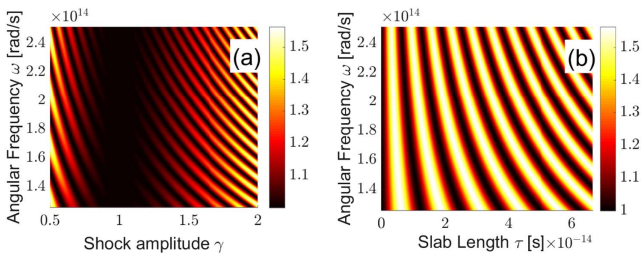

Fig. 7. Analytical transmittance T_{slab} [Eq. (11)] with $E_{\text{F0}} = 0.6$ eV as a function of ω and (a) γ ($\tau = 1.67 \times 10^{-13}$ s) or (b) τ ($\gamma = 2$).

Using the highly tunable framework of graphene, we describe the behavior of plasmons at temporal interfaces. Our analytical approach leads to very simple relations for reflectance and transmittance, which are in very good agreement with rigorous simulations. These results show that energy is injected via a temporal slab into the plasmons. This process is highly tunable via the duration, shock height, and plasmon frequency. In this Letter, we used a Drude dispersion: we did not take into account the detailed microscopic dynamics of the carriers, particularly at the time interface, which is a subject for future studies. Possible applications include frequency selective filters, amplifiers, and modulators. The phenomenon is very general, and our analysis can be adjusted for other guided mode resonances, plasmonic or not.

Funding. Fonds pour la Formation à la Recherche dans l'Industrie et dans l'Agriculture (FRIA).

REFERENCES

1. F. Wang, Y. Zhang, C. Tian, C. Girit, A. Zettl, M. Crommie, and Y. R. Shen, Science **320**, 206 (2008).
2. L. Ren, Q. Zhang, J. Yao, Z. Sun, R. Kaneko, Z. Yan, S. Nanot, Z. Jin, I. Kawayama, M. Tonouchi, J. M. Tour, and J. Kono, Nano Lett. **12**, 3711 (2012).
3. T. Low and P. Avouris, ACS Nano **8**, 1086 (2014).
4. E. J. Reed, M. Soljacic, and J. D. Joannopoulos, Phys. Rev. Lett. **91**, 133901 (2003).
5. M. Notomi and S. Mitsugi, Phys. Rev. A **73**, 051803 (2006).
6. S. F. Preble, Q. Xu, and M. Lipson, Nat. Photonics **1**, 293 (2007).
7. M. T. Wade, X. Zeng, and M. A. Popovic, Opt. Lett. **40**, 107 (2015).
8. V. Ginis, P. Tassin, T. Koschny, and C. M. Soukoulis, Phys. Rev. B **91**, 161403 (2015).
9. G. Altares Menendez and B. Maes, Phys. Rev. B **95**, 144307 (2017).
10. Z. Yu and S. Fan, Nat. Photonics **3**, 91 (2009).
11. M. Castellanos Muñoz, A. Y. Petrov, L. O'Faolain, J. Li, T. F. Krauss, and M. Eich, Phys. Rev. Lett. **112**, 053904 (2014).
12. K. Fang, Z. Yu, and S. Fan, Nat. Photonics **6**, 782 (2012).
13. L. Lu, J. D. Joannopoulos, and M. Soljacic, Nat. Photonics **8**, 821 (2014).
14. F. Morgenthaler, IEEE Trans. Microwave Theory Tech. **6**, 167 (1958).
15. V. Bacot, M. Labousse, A. Eddi, M. Fink, and E. Fort, Nat. Phys. **12**, 972 (2016).
16. A. N. Grigorenko, M. Polini, and K. S. Novoselov, Nat. Photonics **6**, 749 (2012).
17. L. A. Falkovsky, J. Phys. **129**, 012004 (2008).
18. M. Jablan, H. Buljan, and M. Soljacic, Phys. Rev. B **80**, 245435 (2009).
19. Y. Xiao, D. N. Maywar, and G. P. Agrawal, Opt. Lett. **39**, 574 (2014).
20. M. I. Bakunov and A. V. Maslov, Opt. Lett. **39**, 6029 (2014).
21. D. K. Kalluri, *Electromagnetics of Time Varying Complex Media: Frequency and Polarization*, 2nd ed. (CRC Press, 2010).
22. J. T. Mendoça and P. K. Shukla, Phys. Scripta **65**, 160 (2002).
23. Comsol AB, "Comsol multiphysics v 5.2," www.comsol.com.
24. I. Gierz, J. C. Petersen, M. Mitrano, C. Cacho, I. C. E. Turcu, E. Springate, A. Stöhr, A. Köhler, U. Starke, and A. Cavalleri, Nat. Mater. **12**, 1119 (2013).
25. S. Ulstrup, J. C. Johannsen, F. Cilento, J. A. Miwa, A. Crepaldi, M. Zacchigna, C. Cacho, R. Chapman, E. Springate, S. Mammadov, F. Fromm, C. Raidel, T. Seyller, F. Parmigiani, M. Grioni, P. D. C. King, and P. Hofmann, Phys. Rev. Lett. **112**, 257401 (2014).
26. M. Trushin, A. Grupp, G. Soavi, A. Budweg, D. De Fazio, U. Sassi, A. Lombardo, A. C. Ferrari, W. Belzig, A. Leitenstorfer, and D. Brida, Phys. Rev. B **92**, 165429 (2015).
27. G. Altares Menendez, G. Rosolen, and B. Maes, J. Opt. **18**, 125004 (2016).
28. Q. H. Wang, K. Kalantar-Zadeh, A. Kis, J. N. Coleman, and M. S. Strano, Nat. Nanotechnol. **7**, 699 (2012).